Supplementary Information

All-solid-state flexible zinc-air battery with polyacrylamide alkaline gel electrolyte

He Miao[a, b, *], Bin Chen[a], Shihua Li[c], Xuyang Wu[a], Qin Wang[a], Chunfei Zhang[a], Zixu Sun[b], Hong Li[b, *]

[a] Faculty of Maritime and Transportation, Ningbo University, Ningbo 315211, PR China

[b] School of Mechanical and Aerospace Engineering, Nanyang Technological University, Singapore 639798, Singapore

[c] Key Laboratory of Graphene Technologies and Applications of Zhejiang Province, Ningbo Institute of Materials Technology and Engineering, Chinese Academy of Sciences, Zhejiang 315201, PR China

*Corresponding authors:

Prof. He Miao, E-mail: miaohe@nbu.edu.cn

Prof. Hong Li, E-mail: ehongli@ntu.edu.sg

■ Materials

Graphite (80 μm), $KMnO_4$ (AR), KNO_3 (AR), H_2SO_4 (98%), $C_4H_6MnO_4{\cdot}4H_2O$ (AR), $(NH_4)_2S_2O_8$ (AR), urea ($CO(NH_2)_2$, AR), KOH (85.0%), N, N'-methylene-bis-acrylamide (MBA, AR), Acrylamide (AM, AR), H_2O_2 (AR), $K_2S_2O_8$ (AR), polyvinyl alcohol (PVA, AR) and acrylic acid (AA, AR) were purchased from Sinopharm Chemical Reagent Co. Ltd. or Aldrich.

■ Preparation of MnO_2/NRGO, MnO_2/NRGO$_{-140}$, MnO_2/NRGO$_{-160}$, MnO_2/NRGO$_{-0.5}$, MnO_2/NRGO$_{-1}$ and MnO_2/NRGO$_{-5}$

Graphene oxide (GO) was prepared from natural graphite flakes by a modified Hummers method. MnO_2/NRGO was synthesized by hydrothermal assembly of GO, $C_4H_6MnO_4{\cdot}4H_2O$ and $(NH_4)_2S_2O_8$ combining with freeze-drying. Briefly, 3 mM $C_4H_6MnO_4{\cdot}4H_2O$ was added into 10 mL deionized water to form a homogeneous solution. 20 mL of GO dispersion (2.5 mg mL^{-1}) was added into the $C_4H_6MnO_4$ solution and stirred thoroughly to form a stable aqueous suspension by sonication for 30 min. Then, 2g $(NH_4)_2S_2O_8$ was dissolved into suspension. Subsequently, the stable suspension was sealed in a Teflon-lined autoclave and hydrothermally treated for 12 h at 180 °C, respectively. The products were washed with deionized water for many times, and then freeze-dried for 48 hours to obtain MnO_2/NRGO.

MnO_2/NRGO$_{-140}$, MnO_2/NRGO$_{-160}$, MnO_2/NRGO$_{-0.5}$, MnO_2/NRGO$_{-1}$ and MnO_2/NRGO$_{-5}$ were prepared with the same preparation process of MnO_2/NRGO except for the hydrothermal temperature of 140 and 160 ^oC and Mn^{2+} molar concentrations of 0.5, 1 and 5 mM, respectively.

■ Preparation of NRGO

For preparing NRGO, 20mL GO solution (2.5 mg mL^{-1}) was added into 10 mL deionized water to form a stable aqueous suspension by sonication for 30 min. Then, 1.5 g urea was dissolved into the suspension by sonication. Subsequently, the suspension was sealed in a Teflon-lined autoclave and hydrothermally treated at 180 °C for 12 h. Lastly, the products were washed by deionized water for many times, and then freeze-dried for 48 hours to obtain NRGO.

■ **Preparation of MnO_2/C**

The synthesis of MnO_2 nanowires/carbon composite (MnO_2/C) was almost same with that of MnO_2/NRGO hydrothermally treated at 180 °C, except that 20 mL of GO dispersion (2.5 mg mL^{-1}) was replaced by 0.05g Vulcan-XC 72 carbon powder.

■ **Preparation of PAM, PVA and PAA-based AGEs**

The preparation of PAM-based AGEs was described as follows: KOH with different weights were dissolved in 13g deionized water to form the alkaline solution with different concentrations. 0.6g N, N'-methylene-bis-acrylamide (MBA) and acrylamide (AM) with different weights were added into 5g deionized water, and kept stirring at 50 ^oC until they completely dissolved. Then, the prepared alkaline solution was mixed with the AM/MBA solution, and kept stirring at 50 ^oC for 30 minutes. Then, the solution was poured into a culture dish. 50 μl $K_2S_2O_8$ solution (5 wt%) was added into the culture dish by dripping under vigorous stirring. After about 10 minutes, the PAM-based AGEs were obtained at room temperature.

The PVA-based AGE was prepared as follows: 1.0 g polyvinyl alcohol (PVA) powder (MW 20500, Aladdin) was dissolved in 10.0 mL deionized water at 90 ^oC under magnetic stirring for 2 h. Then 2.0 mL 18.0 M KOH was added, and the electrolyte solution was kept stirring at 90 ^oC for 1 h. Then the solution was freezed at -20 ^oC over 12 h to improve the mechanical strength of the gel-electrolyte. Finally, put the prepared gel-electrolyte at room temperature.

The PAA-based AGE was prepared as follows: 18 g KOH was dissolved in 26 g deionized water to form the alkaline solution. For the preparation of polymer solution, 0.5 g MBA was added into 3 g acrylic acid (AA) solution, and kept stirring until dissolved. The as-prepared alkaline solution and polymer solution were mixed and kept stirring for 5 min. The clear mixing solution was poured into a culture dish. 50 ul $K_2S_2O_8$ solution (5 wt%) was added into the culture dish by dripping under vigorous stirring. Finally, put the prepared gel-electrolyte at room temperature.

■ **Material characterization**

X-ray diffraction (XRD) patterns were obtained on a Bruker D8 Advance X-ray diffract meter (Cu Kα = 1.5418 Å) at a scanning rate of 0.02° s^{-1} from 10° to 80°. The

microstructures of the synthesized samples were observed using a field-emission scanning electron microscopy (FESEM, Hitachi S4800, 5kV). The Brunauer-Emmett-Teller (BET) specific surface areas of the samples were measured and analyzed by means of Micromeritics ASAP 2020M instrument. X-ray photoelectron spectroscopy (XPS) data were obtained on an AXISULTARDLD spectroscopy spectrometer with an Al-Kα X-ray source.

■ **Preparation of working electrode**

The working electrode was prepared as follows: the catalyst inks were prepared by dispersing 5 mg catalysts and 5 mg carbon (Vulcan-XC72) in 2 mL absolute ethanol, and then 80 μL 5 wt% Nafion solution (DuPont) was added and ultrasonically blended for 1h to form a well-dispersed ink. 20 μL catalyst ink was carefully dropped onto the glassy carbon electrode (5 mm in diameter) with the electrocatalyst loading of 255 μg cm^{-2}. The working electrodes were then dried in air at room temperature for 1 hour.

■ **Measurement of working electrode**

Cyclic voltammetry (CV), linear sweep voltammetry (LSV) curves of ORR and OER were recorded at +0.4 ~ -0.8 V, +0.2 ~ -0.8 V and +0.2 ~ 1.0 V (vs. Hg/HgO) at a scan rate of 5 mV s^{-1}, respectively. LSV data of ORR and OER were obtained with rotating electrode speeds at 1600 rpm with an iR (R = 47 Ω) correction. A fixed voltage of 1.4 V (vs. RHE) was applied to the ring electrode to investigate the amount of peroxide generated from the disk electrode during ORR. The percentages of HO_2^- ($X(HO_2^-)$) and transferred electron numbers (n_e-) can be calculated by the ring current (I_{ring}), disk current (I_{disk}) and ring collection efficiency (N) obtained from RRDE by Eqs. (1) and (2), respectively.

$$n = \frac{4I_d}{I_d + (\frac{I_{ring}}{N})} \quad (1)$$

$$X_{HO_2^-}[\%] = 100\frac{\frac{2I_{ring}}{N}}{I_{disk} + (\frac{I_{ring}}{N})} \quad (2)$$

Chronoamperometry (CA) and chronopotentiometry (CP) techniques were

applied to assess the durabilities of the different catalysts toward ORR and OER in 0.1 mol L^{-1} KOH O_2-saturated electrolyte, respectively, and the rotation rate of RDE was fixed at 1600 rpm.

■ **Measurement and calculation of ionic conductivity**

The ionic conductivity of AGE was calculated by the ohmic resistance obtained from AC impedance spectra measurement over a frequency ranging from 100 kHz to 0.1 Hz with an amplitude of 5 mV on an electrochemical workstation (CHI 760E). The ionic conductivity (σ) was calculated as follows:

$$\sigma = \frac{l}{RA} \tag{3}$$

where σ, l, R, and A represent the conductivity, thickness, bulk resistance, and area of gel polymer electrolyte, respectively.

■ **Test of the ZABs**

All the battery tests were performed on a multi-channel battery test system (LAND CT2001A, Wuhan LAND Electronic Co., Ltd, China) at room temperature. I-V curves of the batteries under charge/discharge were obtained at the different current densities. The cyclic stability of ZAB was measured at the current density of 5 mA cm^{-2} with 10 min per cycle (5 min charge and 5 min discharge). The specific capacity (mAh g^{-1}) of ZAB was tested at the current density of 10 mA cm^{-2} and calculated by the following equation.

$$C = \frac{It \times 1000}{m \times 3600} \tag{4}$$

Where C, I, t and m represent specific capacity (mAh g^{-1}), current (A), service hours (s) and weight of consumed zinc (g), respectively.

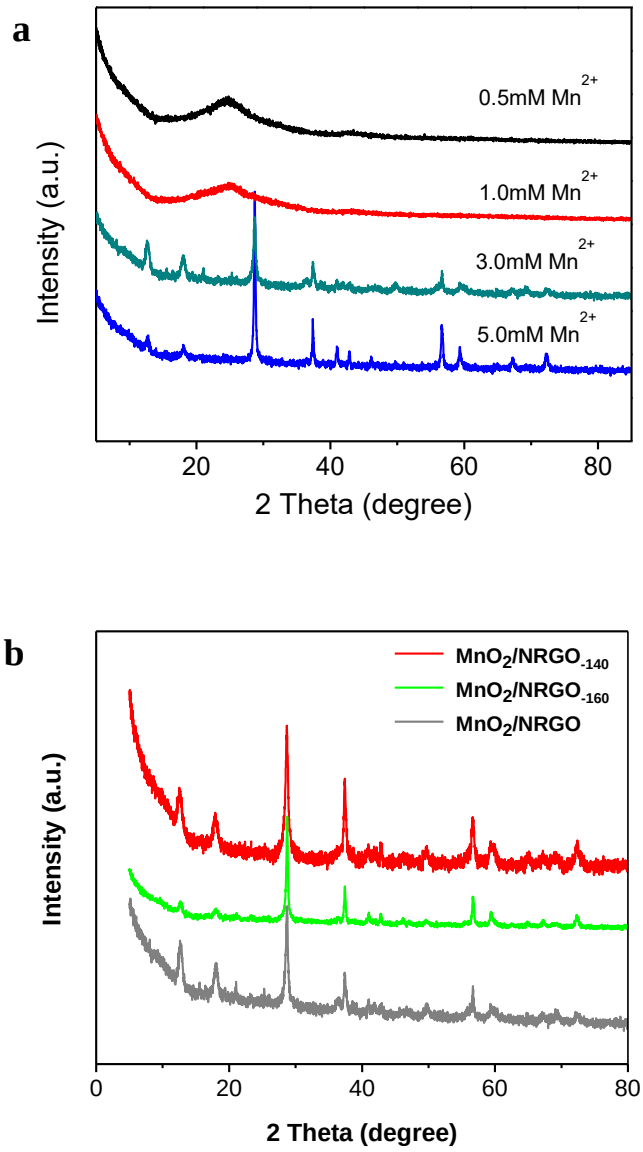

Fig. S1 XRD patterns of (a) $MnO_2/NRGO_{-0.5}$, $MnO_2/NRGO_{-1}$, $MnO_2/NRGO$, $MnO_2/NRGO_{-5}$ and (b) $MnO_2/NRGO_{-140}$, $MnO_2/NRGO_{-160}$, $MnO_2/NRGO$.

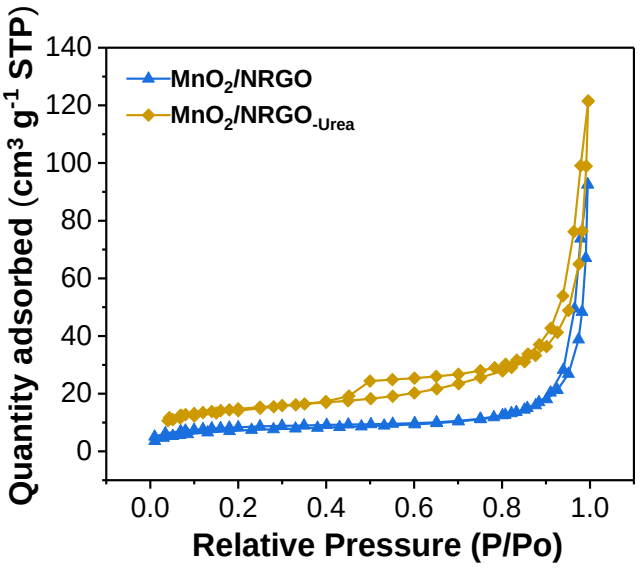

Fig. S2 N_2 adsorption/desorption isothermal curves of MnO_2/NRGO and MnO_2/NRGO-$_{Urea}$.

The specific surface area of MnO_2/NRGO-$_{Urea}$ and MnO_2/NRGO are 51 m^2 g^{-1} and 45 m^2 g^{-1}, respectively.

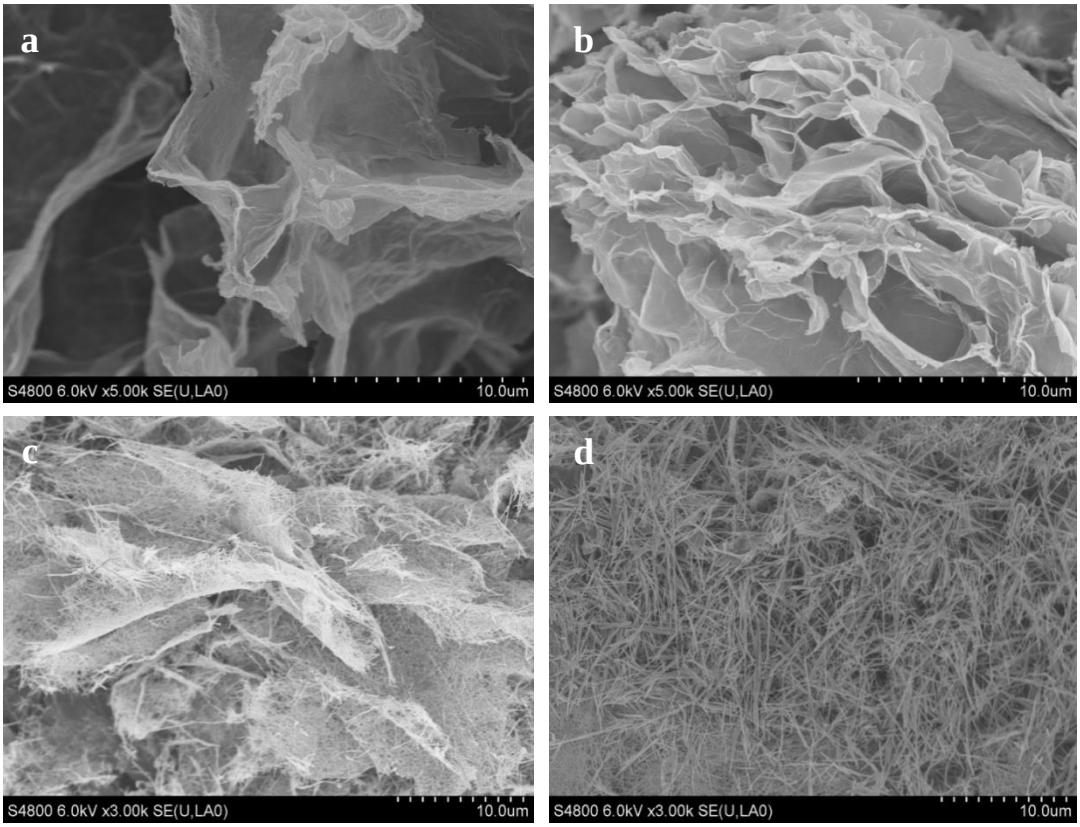

Fig. S3 SEM images of MnO_2/NRGO$_{-0.5}$, MnO_2/NRGO$_{-1}$, MnO_2/NRGO and MnO_2/NRGO$_{-5}$.

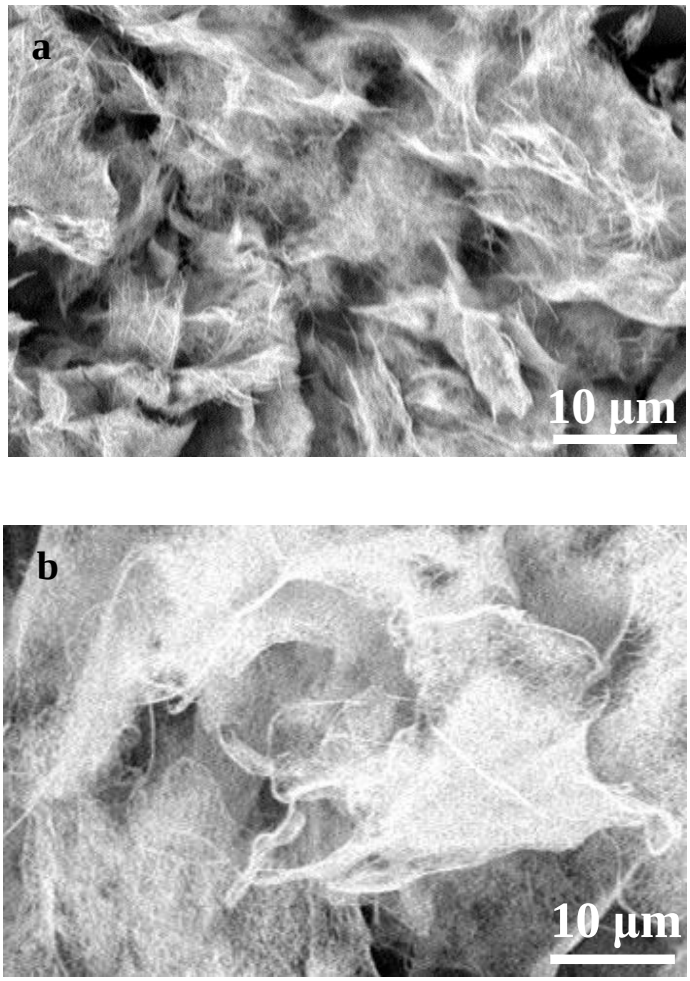

Fig. S4 SEM images of (a) MnO_2/NRGO$_{-140}$ and (b) MnO_2/NRGO$_{-160}$.

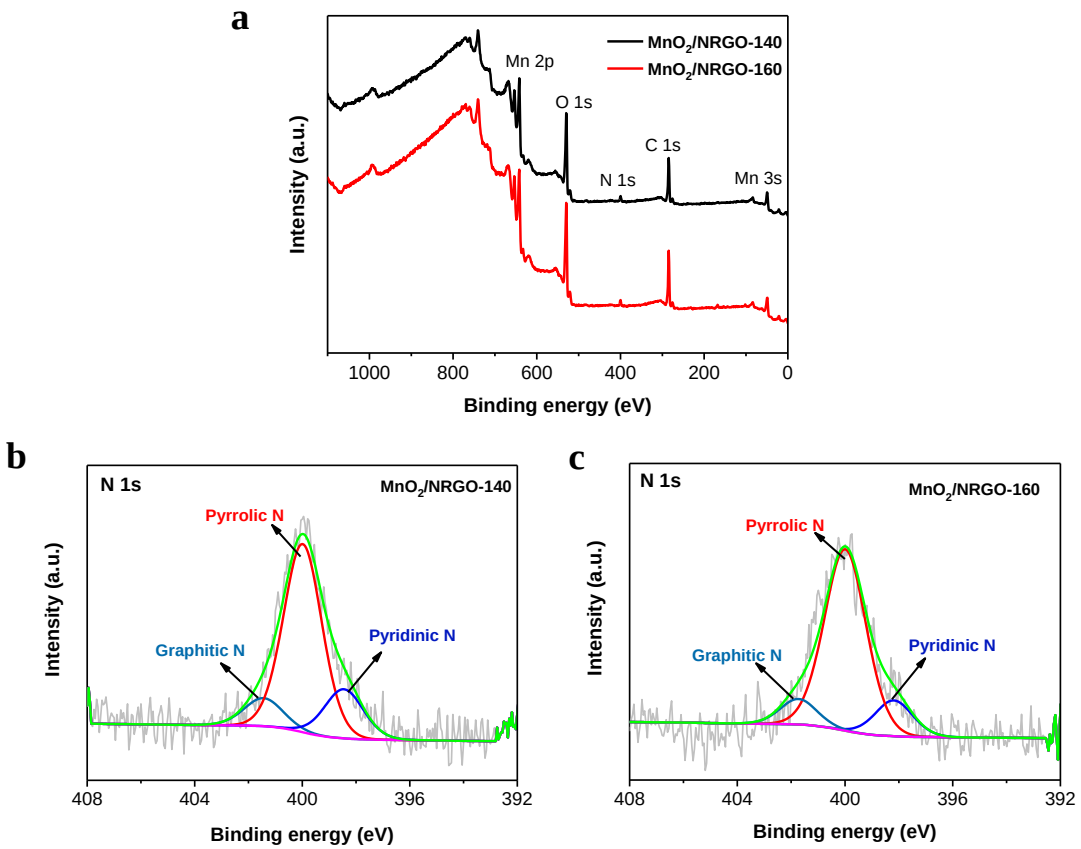

Fig. S5 (a) XPS spectrums of synthesized samples. (b) High resolution N 1s spectra of MnO_2/NRGO$_{-140}$ and MnO_2 /NRGO$_{-160}$.

By increasing the hydrothermal temperature from 140 to 180 ^oC, the N content in the as-prepared catalyst also can be slightly enhanced. Based on the simulations of N1s peak in the XPS curves, it can be readily found that pyrrolic N is dominant among the three N nitrogen configurations in the MnO_2/NRGO$_{-140}$ and MnO_2/NRGO$_{-160}$.

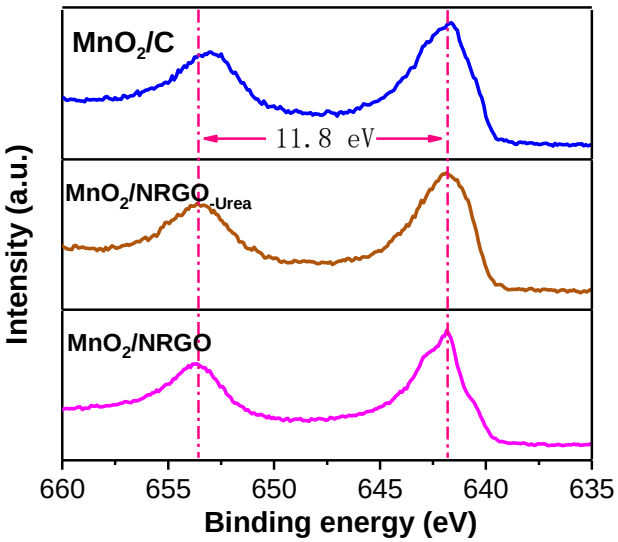

Fig. S6 High resolution Mn 2p XPS spectra of MnO_2, MnO_2/C, MnO_2/ NRGO and MnO_2/NRGO$_{-Urea}$ catalysts.

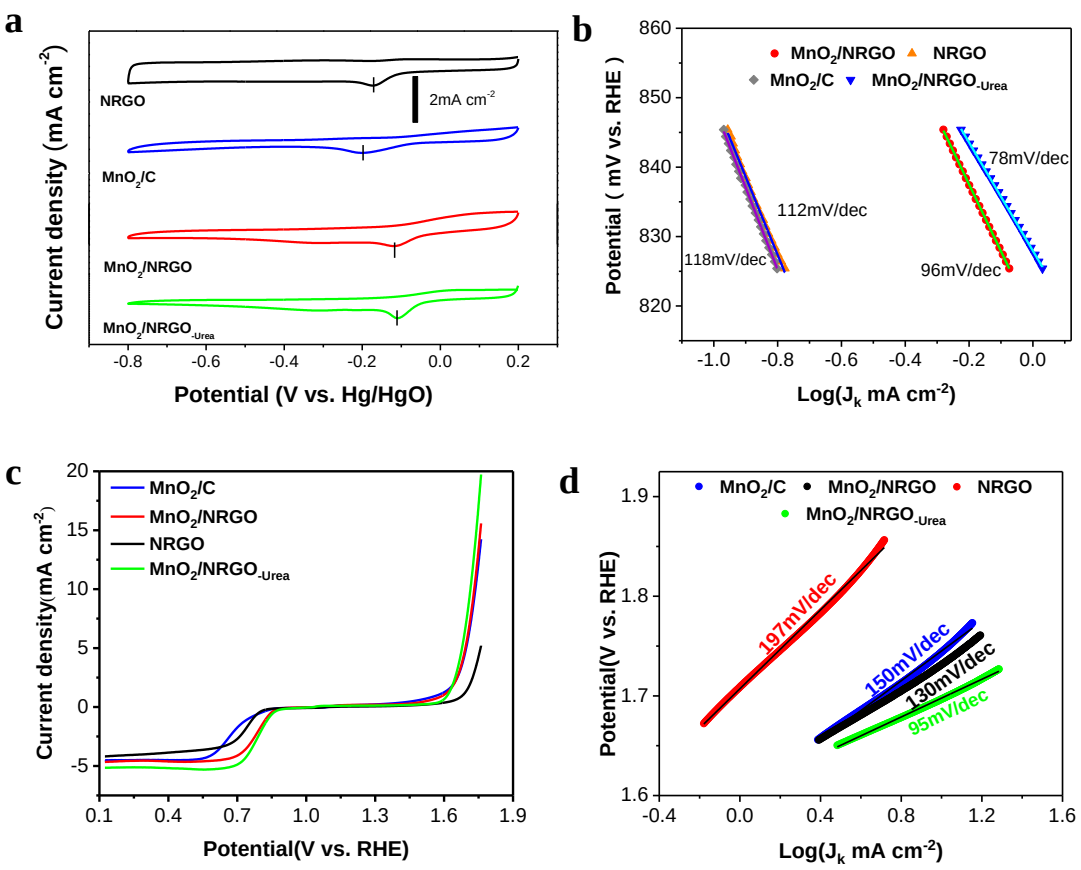

Fig. S7 Electrochemical properties of the as-prepared samples. (a) ORR CV curves. (b) Tafel plots derived from ORR LSV curves. (c) Overall polarization curves of catalysts within the ORR and OER potential window. (d) Tafel plots derived from OER LSV curves. Electrolyte: O_2-saturated 0.1M KOH solution; rotation rate: 1600 rpm; scan rate: 5 mVs^{-1}.

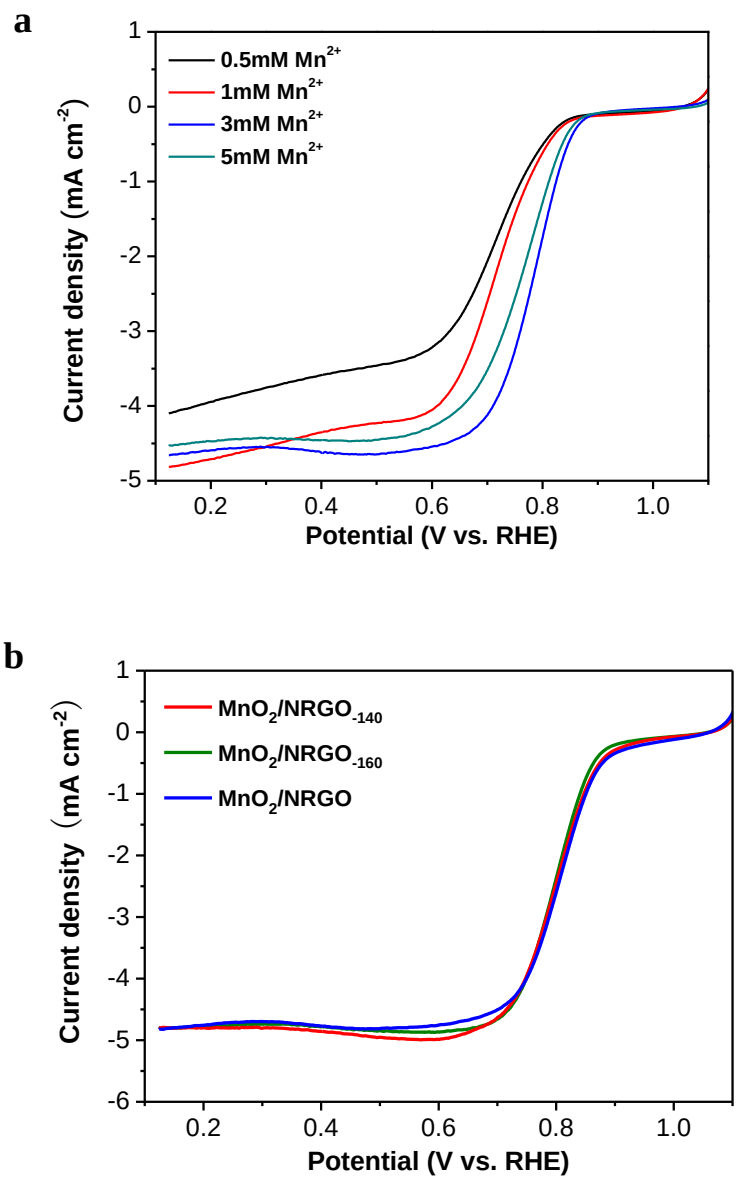

Fig. S8 ORR LSV curves of (a) $MnO_2/NRGO_{-0.5}$, $MnO_2/NRGO_{-1}$, $MnO_2/NRGO$, $MnO_2/NRGO_{-5}$ and (b) $MnO_2/NRGO_{-140}$, $MnO_2/NRGO_{-160}$, $MnO_2/NRGO$.

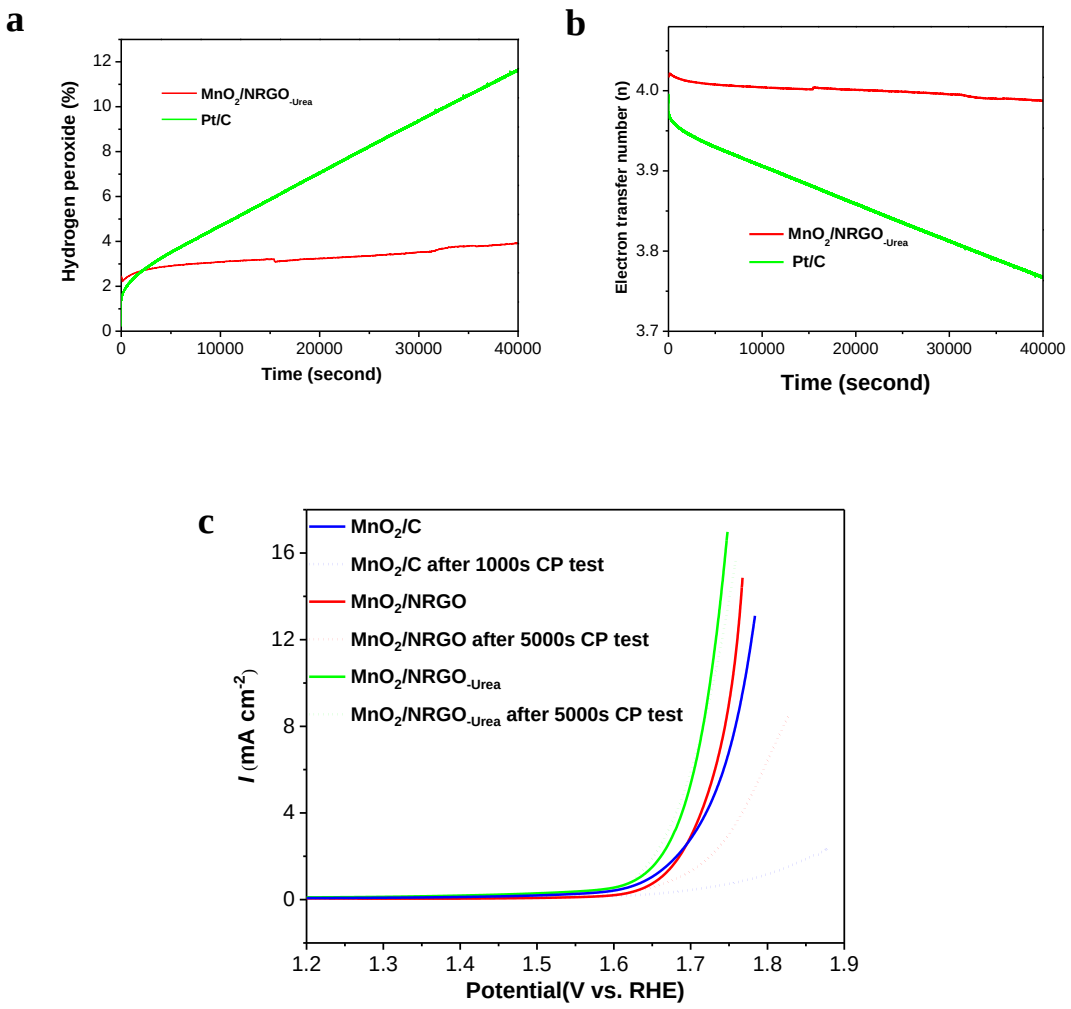

Fig. S9 Long-term stabilities of the as-prepared samples: (a) *X* (HO_2^-) and (b) transferred electron number (n_{e^-}) versus time of MnO_2/NRGO-Urea and Pt/C. (c) OER LSV curves of MnO_2/C, MnO_2/NRGO and MnO_2/NRGO-Urea before and after CP test.

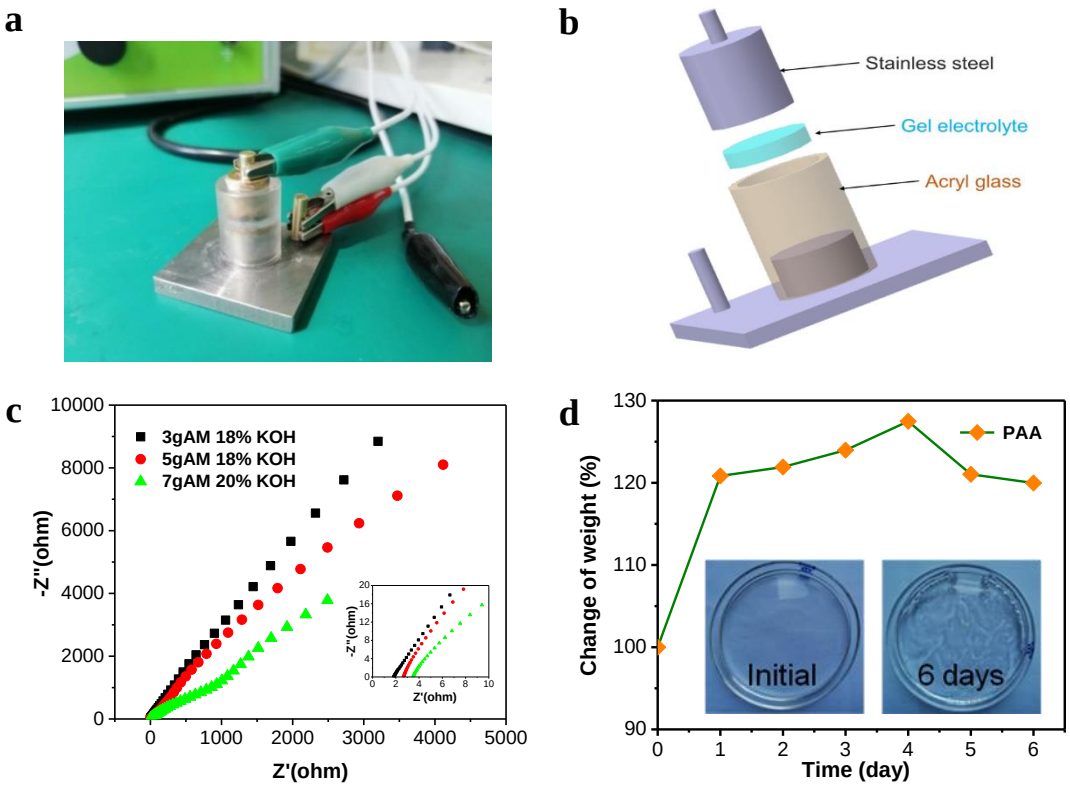

Fig. S10 (a) Photograph and (b) schematic diagram of the homemade device for testing the ionic conductivities of AGEs. (c) EIS plots of the three representative PAM-based AGEs. (d) Weight change of PAA-based AGEs. Insets are the photographs of the PAA-based AGE exposed in the ambient air environment.

When PAA-based AGE is exposed in the ambient air environment, it expands obviously and its surface becomes uneven. After 6 days, the weight of PAA-based AGE increases by ~20%. This indicates that PAA-based AGE is not suitable for the all-solid-state flexible ZABs.

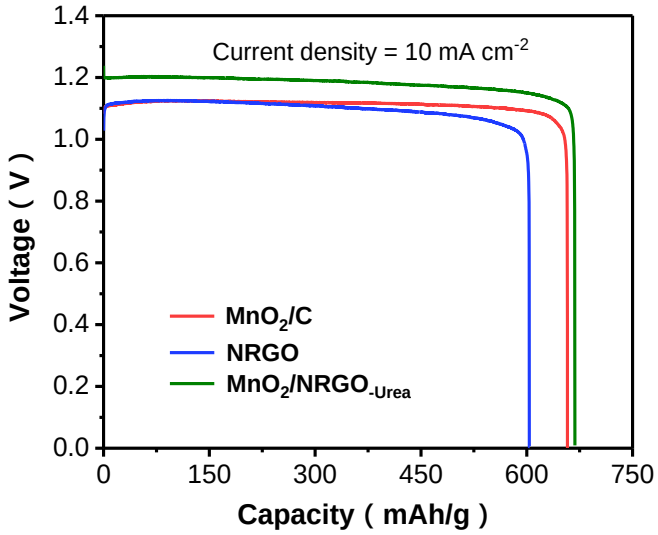

Fig. S11 Discharge curves of the flexible ZABs with different catalysts and PAM-based AGE at a constant current density of 10 mA cm^{-2}.

Table S1 Atomic percentages of Mn, C, O and N in the different catalysts from XPS analyses.

Samples	Mn (at%)	C (at%)	O (at%)	N (at%)
MnO_2/NRGO	12.8	46.3	37.9	3.0
MnO_2/NRGO-$_{Urea}$	18.0	35.2	43.3	3.5
MnO_2/NRGO-$_{160}$	13.7	42.7	40.8	2.8
MnO_2/NRGO-$_{140}$	16.3	42.6	38.5	2.6

Table S2 Comparison of ORR and OER bifunctional activities and stabilities of MnO_2/NRGO-Urea with comparative manganese oxide based catalysts in literatures.

Catalysts	$E_{1/2}$ (V vs. RHE)	$E_{j=10}$ (V vs. RHE)	ΔE (V)	ORR stability (%)	OER stability (%)	references
MnO_2/NRGO-Urea	0.80	1.69	0.89	98%/40000s	negligible	This work
α-MnO_2 nanotube	~0.73	--	--	--	--	[1]
GO-HLMO	~0.63	--	--	--	--	[2]
CoO/MnO_2/RGO	0.76	--	--	--	--	[3]
Ni-MnO/rGO	0.78	1.60	0.82	94%/10000s	14%/10000s	[4]
MnOx4:CoOx1/NG	0.73	1.80	1.07	--	--	[5]
δ-MnO_2/SGS	0.80	--	--	95%/20000s	--	[6]
MnO_2-150-0.5/N-KB	~0.74	1.83	1.09	37mV/5000c	--	[7]
Li-bir/rGO	0.72	1.72	1.0	negligible	--	[8]
α-MnO_2	~0.76	1.72	~0.96	--	--	[9]
Mn_xO_y/NC	~0.75	1.68	~0.93	--	--	[10]
y2Co-NCNT-1Mn	0.75	1.71	0.96	--	--	[11]
50%Ag-MnO_2	0.67	--	--	91%/50000s	--	[12]
17% Ag-MnO_2/C	0.80	--	--	97%/45000s	--	[13]
4.8%Ce-MnO_2/C	0.78	--	--	96%/40000s	--	[14]
Co_3O_4/MnO_2/PQ-7	~0.86	~1.78	~0.92	82%/48000s	--	[15]
$(Fe_2O_3/MnO_2)_{3/4}$-$(CNTs)_{1/4}$	~0.82	>1.7	>0.88	30%/1000c	negligible	[16]
Mn_2O_3 thin film	~0.75	1.77	~1.02	--	--	[17]
N-G@MnO_2-3	0.8	--	--	81%/18000s	--	[18]
Ir/C	0.68	1.62	0.94	--	--	[19]
Pt/C	0.83	1.97	1.14	88%/40000s	--	[19]
Pt/C+RuO_2	0.83	1.88	1.05	--	--	[20]

$E_{1/2}$: Half-wave potential; $E_{j=10}$: OER potential at 10 mA cm^{-2}; ΔE: potential gap between $E_{1/2}$ (ORR) and $E_{j=10}$ (j=10 mA cm^{-2}, OER)

Table S3 Comparison of the ion conductivities of PAM-based AGE with that of the other flexible electrolytes in the all- solid-state ZABs reported recently.

Flexible electrolytes	Temperature	Conductivity (mS cm^{-1})	Reference
PAM	r.t	215.6	This work
A201	r.t	42.0	[21]
QAFCGO	r.t	33.3	[21]
PGG-GP	r.t	123	[22]
2-QAFP-14	r.t	48.3	[23]
GGPE	r.t	3.1	[24]
2-QAFC	r.t	21.2	[25]
PC	r.t	~2	[25]
PDDA33	80 ^{o}C	47.3	[26]
2-BPCE	---	81.7	[27]
PVA	r.t	77.0	[27]
PEO-PVA-glass-fibre-mat	70 ^{o}C	58	[28]
PVA/PAA	r.t	30.1	[29]
Celgard3501	r.t	13.7	[30]
PVdF-HFP	r.t	2.2	[31]
PANa	r.t	170	[32]
Tokuyama A901	r.t	11.4	[15]
PVA-SiO_2	r.t	57.3	[33]
PVA	r.t	15	[34]
PVA/PAA film	r.t	11.2	[35]
PANa-cellulose	r.t	150	[36]
PVA-PEO	r.t	180	[37]

Table S4 Comparison of the maximum power density (P_{max}) of all- solid-state ZABs in this work with that of others reported recently.

Catalysts	Catalyst loading (mg cm^{-2})	Electrolyte	P_{max} (mW cm^{-2})	Reference
MnO_2/NRGO-Urea	1	PAM	105	This work
Co_3O_4/MnO_2/PQ-7	1	Tokuyama A901	45	[15]
Pt/RuO_2	2	PANa	88	[32]
Pt/RuO_2	2	PVA	43	[32]
SilkNC/KB	2	PVA	32.3	[38]
ZFL-D-Co_3O_4/CC	2.1	PVA	65	[39]
N-GCNT/FeCo-3	0.2	PVA	97.8	[40]
N-$NiCo_2O_4$	1	PVA	23	[41]
IrO_2+Pt/C	2	CS-PDDA-OH^-	48.9	[26]
CoNC@GF	1.8	PVA	85.6	[42]
Co_3O_4	1	QAFCGO	50	[21]
Co_3O_4/MnO_2-CNTs	2	Tokuyama	62	[43]
Fe_3C/Fe_2O_3@NGNs	1.5	PVA	28.4	[44]
CoNCNTF/CNF	--	PVA	63	[19]
Co_3O_4	0.3	PVA-SiO_2	62.6	[33]
NC-Co/CoN_x	--	PAA	43.9	[45]
$LaNiO_3$/NCNT+Co_3O_4	1	PVA	28.2	[34]
NC-Co_3O_4-90	--	PAA	82	[46]
Pt/C	--	PAA	95.4	[46]
MnO_x-GCC	--	PAA	32	[47]
CC-AC		PVA	52.3	[48]
FeCo-DHO/NCNTs	2	PVA	60	[20]
Fe-N-C	--	PANa-cellulose	108.6	[36]
Co-NC@Al_2O_3	--	PAA	72.4	[49]
Meso-CoNC@GF	--	PAA	85.6	[42]

References

[1] W. Xiao, D. Wang, X. Lou, J. Phys. Chem. C 114 (2019) 1694-1700.

[2] H.Y. Park, T. J. Shin, H. I. Joh, J. H. Jang, D. Ahn, S. J. Yoo, Electrochem. Commun. 41 (2014) 35-38.

[3] W. Huang, H. Zhong, D. Li, P. Tang, Y. Feng, Electrochim. Acta 173 (2015) 575-580.

[4] G. Fu, X. Yan, Y. Chen, L. Xu, D. Sun, J.M. Lee, Y. Tang, Adv. Mater. 30 (2018) 1704609.

[5] Z. Lu, X. Chen, P. Liu, X. Huang, J. Wei, Z. Ren, S. Yao, Z. Fang, T. Wang, J. Masa, J. Electrochem. Soc. 165 (2018) H580-H589.

[6] H. Begum, M. S. Ahmed, S. Jeon, Electrochim. Acta 296 (2019) 235-242.

[7] M. Wang, K Chen, J. Liu, Q. He, G. Li, F. Li, Catalysts 8 (2018) 138-153.

[8] S. Kosasang, N. Ma, N. Phattharasupakun, M. Sawangphruk, J. Electrochem. Soc. 166 (2019) A1543-A1549.

[9] Y. Meng, W. Song, H. Huang, Z. Ren, S. Chen, S. L. Suib, J. Am. Chem. Soc. 136 (2014) 11452-11464.

[10] J. Masa, W. Xia, I. Sinev, A. Zhao, Z. Sun, S. Grutzke, P. Weide, M. Muhler, W. Schuhmann, Angew. Chem. Int. Ed. 53 (2014) 8508-8512.

[11] Y. J. Oh, J. H. Kim, Y. C. Kang, Chem Eng. J. 373 (2019) 86-94.

[12] S. Sun, H. Miao, Y. Xue, Q. Wang, S. Li, Z. Liu, Electrochim. Acta 214 (2016) 49-55.

[13] S. Sun, H. Miao, Y. Xue, Q. Wang, Q. Zhang, Z. Dong, S. Li, H. Huang, Z. Liu, J. Electrochem. Soc. 164 (2017) F768-F774.

[14] S. Sun, Y. Xue, Q. Wang, H. Huang, H. Miao, Z. Liu, Electrochim. Acta 263 (2018) 544-554.

[15] X. Li, F. Dong, N. Xu, T. Zhang, K. Li, J. Qiao, ACS Appl. Mater. Interfaces 10 (2018) 15591-15601.

[16] N. Xu, X. Li, H. Li, Y. Wei, J. Qiao, Science Bulletin 62 (2017) 1216-1226.

[17] Y. Gorlin, T. F. Jaramillo, J. Am. Chem. Soc. 132 (2010) 13612-13614.

[18] Q. Le, M. Huang, T. Wang, X. Liu, L. Sun, X. Guo, D. Jiang, J. Wang, F. Dong, Y. Zhang, J. Colloid and Interface Sci. 544 (2019) 155-163.

[19] D. Ji, L. Fan, L. Li, N. Mao, X. Qin, S. Peng, S. Ramakrishna, Carbon 142 (2019) 379-387.

[20] M. Wu, Q. Wei, G. Zhang, J. Qiao, M. Wu, J. Zhang, Q. Gong, S. Sun, Adv. Energy Mater. 8 (2018) 1801836.

[21] J. Zhang, J. Fu, X. Song, G. Jiang, H. Zarrin, P. Xu, K. Li, A. Yu, Z. Chen, Adv. Energy Mater. 6 (2016) 1600476.

[22] M. Wang, N. Xu, J. Fu, Y. Liu, J. Qiao, J. Mater. Chem. A 7 (2019) 11257-11264.

[23] C. Lin, S. S. Shinde, X. Li, D.H. Kim, N. Li, Y. Sun, X. Song, H. Zhang, C. H. Lee, S. U. Lee, J.H. Lee, ChemSusChem 11 (2018) 3215-3224.

[24] J. Park, M. Park, G. Nam, J.S. Lee, J. Cho, Adv. Mater. 27 (2015) 1396-1401.

[25] J. Fu, J. Zhang, X. Song, H. Zarrin, X. Tian, J. Qiao, L. Rasen, K. Li, Z.i Chen, Energy Environ. Sci. 9 (2016) 663-670.

[26] Y. Wei, M. Wang, N. Xu, L. Peng, J. Mao, Q. Gong, J. Qiao, ACS Appl. Mater. Interfaces 10 (2018) 29593-29598.

[27] N. Zhao, F. Wu, Y. Xing, W. Qu, N. Chen, Y. Shang, M. Yan, Y. Li, L. Li, R. Chen, ACS Appl. Mater. Interfaces 11 (2019) 15537-15542.

[28] C. Yang, S.J. Lin, J. of Power Sources 112 (2002) 497-503.

[29] G. M. Wu, S. J. Lin, C. C. Yang, J. Membr. Sci. 280 (2006) 802-808.

[30] H.J. Lee, J.M. Lim, H.W. Kim, S.H. Jeong, S.W. Eom, Y. T. Hong, S.Y. Lee, J. Membr. Sci. 499 (2016) 526-537.

[31] Z. Liu, S. Z. E. Abedin, F. Endres, J. Solid State Electrochem. 18 (2014) 2683-2691.

[32] Y. Huang, Z. Li, Z. Pei, Z. Liu, H. Li, M. Zhu, J. Fan, Q. Dai, M. Zhang, L. Dai, Adv. Energy Mater. 8 (2018) 1802288.

[33] X. Fan, J. Liu, Z. Song, X. Han, Y. Deng, C. Zhong, W. Hu, Nano Energy 56 (2019) 454-462.

[34] J. Fu, D. U. Lee, F. M. Hassan, L. Yang, Z. Bai, M. G. Park, Z. Chen, Adv. Mater. 27 (2015) 5617-5622.

[35] H.W. Kim, J.M. Lim, H.J. Lee, S.W. Eom, Y. T. Hong, S.Y. Lee, J. Mater. Chem. A 4 (2016) 3711-3720.

[36] L. Ma, S. Chen, D. Wang, Q. Yang, F. Mo, G. Liang, N. Li, H. Zhang, J. A. Zapien, C. Zhi, Adv. Energy Mater. 9 (2019) 1803046.

[37] Y. Xu, Y. Zhao, J. Ren, Y. Zhang, H. Peng, Angew. Chem. Int. Ed. 55 (2016) 7979-7982.

[38] C. Wang, N.H. Xie, Y. Zhang, Z. Huang, K. Xia, H. Wang, S. Guo, B. Xu, Y. Zhang, Chem. Mater. 31 (2019) 1023-1029.

[39] Y. Zhong, Z. Pan, X. Wang, J. Yang, Y. Qiu, S. Xu, Y. Lu, Q. Huang, W. Li, Adv. Sci. 6 (2019) 1802243.

[40] C. Su, H. Cheng, W. Li, Z. Liu, N. Li, Z. Hou, F. Bai, H. Zhang, T. Ma, Adv. Energy Mater. 7 (2017) 1602420.

[41] J. Bian, X. Cheng, X. Meng, J. Wang, J. Zhou, S. Li, Y. Zhang, C. Sun, ACS Appl. Energy Mater. 2 (2019) 2296-2304.

[42] S. Liu, M. Wang, X. Sun, N. Xu, J. Liu, Y. Wang, T. Qian, C. Yan, Adv. Mater., 30 (2018) 1704898.

[43] N. Xu, Y. Liu, X. Zhang, X. Li, A. Li, J. Qiao, J. Zhang, Scientific Reports 6 (2016) 33590.

[44] Y. Tian, L. Xu, J. Qian, J. Bao, C. Yan, H. Li, H. Li, S. Zhang, Carbon 146 (2019) 763-771.

[45] C. Guana, A. Sumboja, W. Zang, Y. Qian, H. Zhang,X. Liu, Z. Liu, D. Zhao, S. J. Pennycook, J. Wang, Energy Storage Mater. 16 (2019) 243-250.

[46] C. Guan, A. Sumboja, H. Wu, W. Ren, X. Liu, H. Zhang, Z. Liu, C. Cheng, S. J. Pennycook, J. Wang, Adv. Mater. 29 (2017) 1704117.

[47] A. Sumboja, M. Lübke, Y. Wang, T. An, Y. Zong, Z. Liu, Adv. Energy Mater. 7 (2017) 1700927.

[48] K. Kordek, L. Jiang, K. Fan, Z. Zhu, L. Xu, M. Al-Mamun, Y. Dou, S. Chen, P. Liu, H. Yin, P. Rutkowski, H. Zhao, Adv. Energy Mater. 9 (2019) 1802936.

[49] L. Zhu, D. Zheng, Z. Wang, X. Zheng, P. Fang, J. Zhu, M. Yu,Y. Tong, X. Lu, Adv. Mater. 30 (2018) 1805268.